Nano Energy 76 (2020) 105081

Contents lists available at ScienceDirect

Nano Energy

journal homepage: http://www.elsevier.com/locate/nanoen

On the chemistry of grain boundaries in $CuInS_2$ films

Torsten Schwarz [a,*], Alberto Lomuscio [b], Susanne Siebentritt [b], Baptiste Gault [a]

[a] Max-Planck-Institut für Eisenforschung GmbH, Max-Planck-Straße 1, 40237, Düsseldorf, Germany
[b] Laboratory for Photovoltaics, Physics and Materials Science Research Unit, University of Luxembourg, Belvaux, Luxembourg

ARTICLE INFO

Keywords:
Thin-film solar cells
CIGS
Grain boundaries
Impurity segregation
Atom probe tomography (APT)
Transmission kikuchi diffraction (TKD)

ABSTRACT

We conducted correlated transmission Kikuchi diffraction and atom probe tomography measurements to investigate the relationship between the structure and chemistry of grain boundaries in Cu-rich and Cu-poor sulfide chalcopyrite $CuInS_2$ thin-films. We detect different elemental redistributions at random high-angle grain boundaries, Σ9 twin boundaries and stacking faults in the Cu-rich and Cu-poor film but no chemical fluctuations at Σ3 twin boundaries. For the Cu-rich $CuInS_2$ thin-film, our atom probe tomography analyses reveal Cu enrichment as well as In and S depletion at random grain boundaries, Σ9 twin boundaries and stacking faults. Hence, we may observe a 'Cu on In' scenario, which is accompanied by co-segregation of Na and C. In contrast, for the Cu-poor $CuInS_2$ thin-film, our analyses show Cu depletion and In enrichment at random grain boundaries and at the vast majority of stacking faults. For S we do not observe a clear trend. Therefore, for the Cu-poor $CuInS_2$ thin-film we may observe a 'In on Cu' scenario, which is accompanied by co-segregation of Na, K and O at the random grain boundaries but not at stacking faults. The amount of impurity segregation varies from one grain boundary to another in both thin-films.

1. Introduction

Sulfide chalcopyrites $Cu(In,Ga)S_2$ (CIGS) are a promising candidate as top junction in stacked tandem solar cells, which have the potential to achieve solar energy conversion efficiencies beyond 30% by overcoming the Shockley-Queisser limit [1]. CIGS has a direct band gap, which can be tuned from 1.55 eV to 2.4 eV for pure $CuInS_2$ and $CuGaS_2$, respectively [2]. Hence, CIGS is suitable to cover the high-energy part of the solar spectrum and it can be current-matched with a bottom junction by controlling its [In]/[Ga] ratio. Recently, CIGS based solar cells achieved a certified record efficiency of 15.5% [3]. However, this value is still far below the 23.35% record efficiency of $Cu(In,Ga)(Se,S)_2$ based solar cells [4].

One main reason for the lower efficiencies for CIGS based solar cells is their high loss in the open-circuit voltage V_{OC}, i.e. the difference of E_g/q - V_{OC}, where E_g is the band gap and q the electric charge. For the certified CIGS based record cell with 15.5% efficiency, a loss in V_{OC} of 630 mV is measured [3]. In contrast, for highly efficient CIGSe based solar cells the V_{OC} loss is approx. 430 mV, i.e. 200 mV smaller compared to pure sulfide CIGS [5–7]. The larger V_{OC} loss for CIGS based solar cells is due to higher recombination activities, which can occur in the bulk of the absorber, at the interface between absorber and back contact as well as between absorber and buffer layer. Indeed, the CIGS absorber and commonly used CdS buffer show an unfavorable cliff-like alignment of their conduction band minima, which causes dominant recombinations at this interface [8,9]. Although alternative buffer materials like Zn(O,S) would allow to overcome this issue by a spike-like band alignment, there is no significant improvement in V_{OC} [10,11]. The quasi Fermi level splitting (QFLS) is an indicator for the recombination activity of the absorber and an upper limit for the V_{OC}. Lomuscio et al. [12] showed that Cu-rich grown $CuInS_2$ (CIS) absorber have a higher QFLS than Cu-poor ones. Cu-rich grown $CuInS_2$ refers to absorber films that were grown under Cu-excess, where a nearly stoichiometric chalcopyrite forms together with a Cu sulfide secondary phase, whereas Cu-poor films are grown with a lower Cu concentration and form the chalcopyrite phase with a reduced Cu content [13]. Final devices based on Cu-rich grown absorbers showcase that the higher QFLS does not result into a higher V_{OC} compared to the Cu-poor grown counterpart. This is related to shunting problems and recombination losses at the interface between the absorber and the buffer [14]. However, if these problems can be overcome, it is essential to know how the QFLS and, hence, the V_{OC} depend on the microstructure of the bare absorber for both Cu-rich and Cu-poor grown $CuInS_2$ absorber films in order to guide their optimization.

* Corresponding author.
E-mail address: schwarz@mpie.de (T. Schwarz).

https://doi.org/10.1016/j.nanoen.2020.105081
Received 30 April 2020; Received in revised form 10 June 2020; Accepted 11 June 2020
Available online 22 June 2020
2211-2855/© 2020 Elsevier Ltd. All rights reserved.

Therefore, as the CIGS absorber layer is a polycrystalline thin-film, one needs to investigate the crystallography and chemistry of extended defects in the CIGS absorber, namely random high-angle grain boundaries (RHAGB), $\sum$3 twin boundaries ($\sum$3 TB) as well as stacking faults (SF) and dislocations. These defects can comprise deep traps within the band gap, which may cause non-radiative Shockley-Read-Hall recombination. Furthermore, charged defects at grain boundaries cause band bending, which limits the QFLS in the absorber [15]. Therefore, these defects can limit the V_{OC} due to an increased saturation current J_0.

For the pure Cu-poor selenides CIGSe, it seems that the GBs are mostly electrically benign. Abou-Ras et al. [16] proposed that an atomic redistribution takes place at GBs, which reduces excess charges and removes deep defects within the band gap. This atomic redistribution at GBs was observed by several groups [16–18]. However, for the pure sulfides CIGS – neither for Cu-poor nor for Cu-rich CIGS – there is nothing known about the chemistry of RHAGBs or $\sum$3 TBs or that of SFs and dislocations.

Therefore, in this study we want to elucidate the chemistry-structure relationships for extended defects in both Cu-rich and Cu-poor grown pure sulfide CIGS based absorbers. For simplicity, we focus only on the ternary system $CuInS_2$ (CIS) to avoid possible phase segregation with the Ga based alloy [19] as well as to avoid a possible influence of a Ga gradient on the chemistry of extended defects. We conduct correlated transmission Kikuchi diffraction (TKD) and atom probe tomography (APT) measurements to provide crystallographic and chemical information on selected GBs at the near atomic scale. Besides GBs, we also present chemical information of SFs and dislocations. We discuss the chemical fluctuations observed at the investigated extended defects and their possible effect on the solar cell performance.

2. Material and methods

The CIS thin-films studied in this work were fabricated in a high vacuum system by co-evaporation of Cu, In and S onto a Mo-coated soda-lime glass (SLG) substrate without a Na barrier layer. One sample was grown under Cu-rich ([Cu]/([In]) = 1.83) conditions at 590 °C and one under Cu-poor ([Cu]/([In]) = 0.95) conditions at 600 °C [14]. Both samples were deposited with constant elemental fluxes in a one-stage-type process, i.e. in particular the Cu-poor CIS thin-film was not subject to a Cu-rich step. The overall composition was measured by EDX in a scanning electron microscope at an acceleration voltage of 20 kV. For the Cu-rich sample, an etching step with 10 wt% KCN for 5 min was applied to remove Cu-S secondary phases [13]. For the Cu-poor sample only a weak etching step with 5 wt% KCN for 30 s was applied in order to clean the surface. Finally, a CdS buffer layer was deposited on both absorber films by chemical bath deposition. Complete cells for current-voltage measurements were fabricated by magnetron sputtering of i-ZnO and Al-doped ZnO and e-beam evaporation of a Ni-Al grid. A summary of all investigated samples is given in Table 1.

The preparation of TEM lamellas and needle-shaped APT specimens was carried out using a dual-beam focused-ion-beam (FIB) (FEI Helios Nanolab 600i), according to the lift-out technique in Ref. [20]. To minimize beam damage due to Ga implantation, a low energy (2–5 keV) Ga beam was used for final shaping of the APT specimens.

STEM-EDX analyses were performed using a JEOL JEM-2200FS TEM equipped with a JEOL EX-24063JGT X-ray detector at an acceleration voltage of 200 kV.

Table 1
List of investigated samples showing the overall composition, growth temperature and whether a KCN etching step was applied or not.

Sample	[Cu]/[In]	T (°C)	KCN etching step
A	1.83	590	10 wt% for 5 min
B	0.95	600	10 wt% for 30 s

TKD measurements were carried out directly on the APT specimens by using a home-built single-tilt TEM retainer [21]. Details of this technique have been described in Ref. [18]. In order to easily distinguish different grains within the TKD datasets, unique grain color maps are used, which assign to each grain a random a unique colour, which is not related to any crystal orientation. APT analyses were performed using a local electrode atom probe (LEAP™ 3000XHR and LEAP™ 5000XR, Cameca Instruments) at a specimen base temperature of 60 K. Measurements were done in pulsed laser mode, using a ~10 ps pulse length, a repetition rate of 100 kHz, and an average detection rate of 4–10 ions per 1000 pulses. For measurements utilizing a laser wavelength of 532 nm and 355 nm we used a laser pulse energy of 100 pJ and 10 pJ, respectively. For the quantification of GB segregation of impurities, Gibbsian interfacial excess values have been determined from ladder diagrams, which are cumulative plots of the number of impurity atoms against the total number of atoms [22].

3. Results

3.1. Microstructure and solar cell parameters

Cross-sectional STEM bright-field (BF) images in Fig. 1 reveal the different microstructures for the CIS thin-films grown under Cu-rich and Cu-poor conditions, respectively. The Cu-rich grown CIS thin-film exhibit grains up to the micrometer range, which contain twin boundaries and stacking faults. Furthermore, we observe smaller sized (<500 nm) grains and voids closer to the Mo back contact. In contrast, for the Cu-poor grown CIS film we find smaller grains, which show signs of dendritic growths and which exhibit a significantly higher density of stacking faults and dislocations. Smaller sized grains (<100 nm) and voids are found close to the Mo back contact as well. Here, the formation of a MoS_2 layer at the back contact is more visible compared to the Cu-rich grown sample (see Fig. S1 in supplementary material). Moreover, the surface roughness is smaller compared to that of the Cu-rich grown one (see also Fig. S1 in supplementary material). STEM-EDX measurements depicted in Fig. 1 reveals the absence of Cu-S compounds on the surface of the Cu-rich grown sample since they were removed by the KCN etching step. However, Cu-S compounds are still detectable in the bulk (see Fig. 1 b)). Interestingly, the surfaces of the voids formed at the Mo back contact are covered with CdS (see Fig. 1 c)). This is likely due to the removal of Cu-S compounds by KCN, which may extend deep into the bulk, and subsequent chemical bath deposition of CdS is filling up the leftover voids and voids being interconnected with them (see Fig. S2 in supplementary material). On the contrary, for the Cu-poor sample we do not detect such a surface coverage of the voids as well as no formation of Cu-S compounds.

Photoluminescence measurements from a previous study [14] of the identical absorber samples show that the QFLS of the Cu-rich grown absorber film yields 839 meV on average and that of the Cu-poor grown one only 670 meV on average. Current-voltage measurements of the complete cells based on the Cu-rich grown sample exhibit severe shunting, which is discussed later. The best solar cell made from the Cu-poor grown sample shows a conversion efficiency η of 8.3%. All cell parameters are summarized in Table 2.

3.2. Cu-rich $CuInS_2$ thin-films

Fig. 2 a-b) shows TKD analyses performed directly on an APT specimen from the Cu-rich sample. The image quality (IQ) values shown in Fig. 2 a), which are a measure of the quality of the Kikuchi pattern, are reduced in the center region of the APT specimen, i.e. darker contrast, due to the presence of a grain boundary. Here, Kikuchi bands from both adjacent grains overlap, which leads to a blurring of the Kikuchi pattern and, hence, to a reduced IQ value. The bottom center region exhibits as well a reduced IQ due to the increasing thickness of the APT specimen. The unique colour map in Fig. 2 b) reveals that the specimen contains

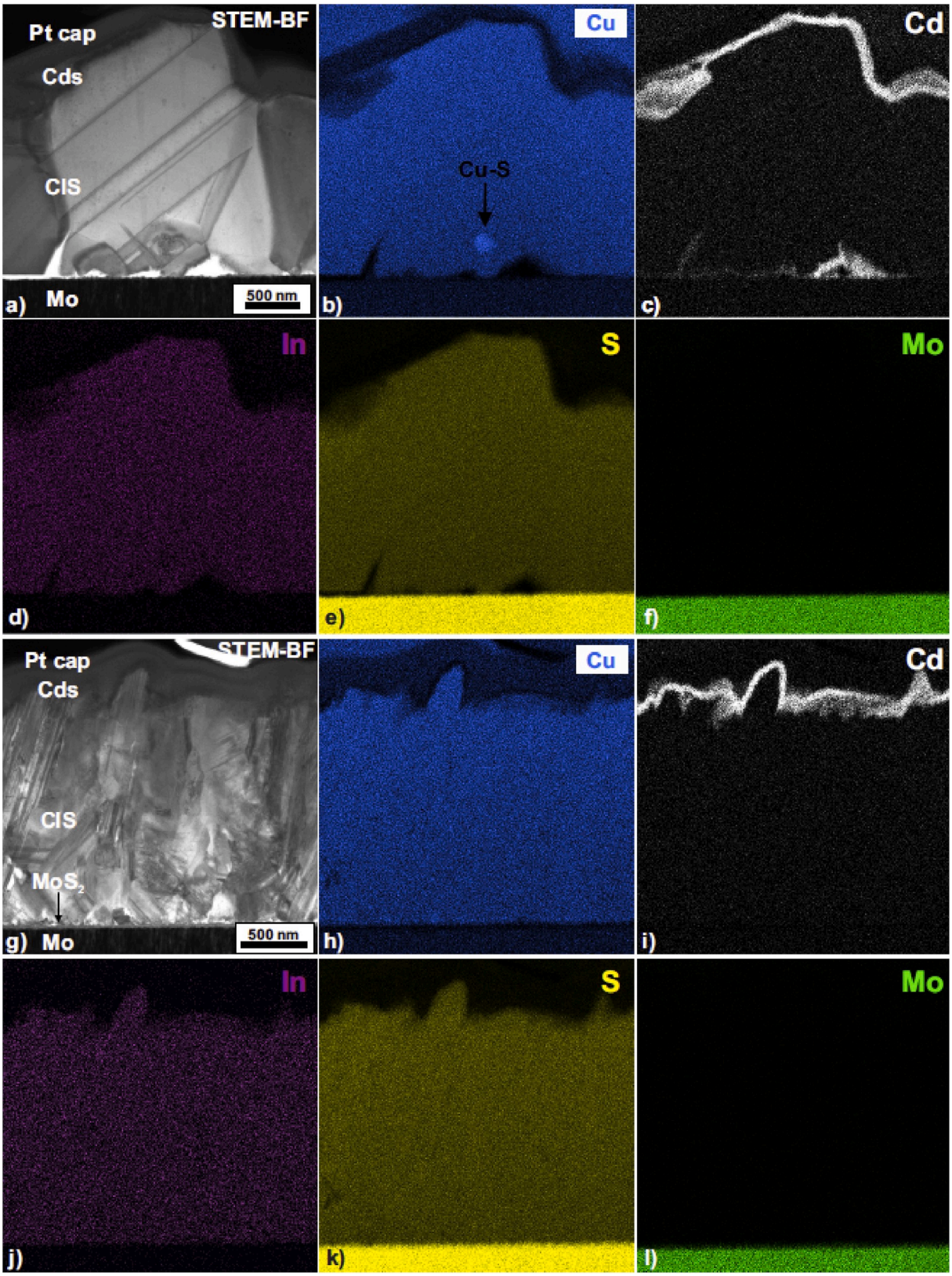

Fig. 1. a-l) Cross-sectional STEM-EDX measurements of the Cu-rich and Cu-poor grown sample. a) and g) show STEM bright-field (BF) images, b) and h) distribution of Cu-K (blue), c) and i) distribution of Cd-L (white), d) and j) the distribution of In-K, e) and k) the distribution of S-L, and f) and l) the distribution of Mo-K for the Cu-rich and Cu-poor grown sample, respectively. Note that the Cu-K line overlaps partly with Pt lines as well as the S-L with Mo lines. Fig. 1 a) is from our previous work [14].

Table 2
List of average QFLS and V_{OC} as well as cell parameters of the best cells. Data from Ref. [14].

Sample	$\overline{QFLS}$ (meV)	$\overline{V_{OC}}$ (mV)	η (%)	V_{OC} (mV)	J_{SC} (mA/cm^2)	FF
Cu-rich	839	–	–	–	–	–
Cu-poor	670	610	8.3	613	20.5	66

one RHAGB (blue line) with a misorientation angle of 26.4° @ [1 1 0] as well as a ∑3 TB (red line). Fig. 2 c) displays the corresponding reconstructed APT dataset showing the Na and C distribution. One can clearly see co-segregation of Na and C at the RHAGB. From the composition profile across this RHAGB in Fig. 2 d) the Gibbsian interfacial excess values for Na and C are calculated to be $\Gamma_{Na} = 0.17$ atoms/nm^2 and $\Gamma_C = 0.05$ atoms/nm^2, respectively. Furthermore, we observe chemical fluctuations of the matrix elements at the RHAGB, namely, Cu enrichment and depletion of In and S. In addition, we detect segregation of mainly Na atoms but also C atoms in clusters (Fig. 2 c)). The composition of Na in those clusters ranges from 0.4 at% to 1.0 at%. Since the APT dataset is not long enough, it does not contain the ∑3 TB given in the TKD analysis. In another APT dataset we observed similar findings for another RHAGB, which is summarized in Table 3.

Fig. 3 a-b) shows the IQ and unique colour map of an APT specimen of the same Cu-rich sample containing a facetted ∑3 TB (red line) and a ∑9 TB (green line). In the corresponding APT dataset in Fig. 3 c) showing the Na and C distribution we observe segregation of C atoms at the ∑9 TB. The composition profile across the ∑9 TB in Fig. 3 d) exhibits that the C composition at this interface is still distinguishable from the background signal ('C-bg' in Fig. 3 d)) and yields an excess value of $\Gamma_C = 0.03$ atoms/nm^2. Interestingly, the compositional fluctuations of the matrix elements are the same as for a RHAGB, i.e. Cu enrichment as well as depletion of In and S. We do not detect any Na segregation at this ∑9 TB.

We detect several Na clusters at the bottom part of the APT dataset, where the location of the ∑3 TB is expected. From an enlarged section of this Na cluster region displayed in Fig. 3 e) we can see that the Na clusters are not homogeneously distributed. The point density map of the identical section shown in Fig. 3 f) reveals that the Na clusters are confined below a sharp line of higher atomic density (orange-red). Comparing Fig. 3 b) and f) clearly exhibit that the inclination angle of the ∑3 TB w.r.t to the black dashed line is the same as for the area with higher atomic density. Although the TKD analyses reveals a facetted ∑3 TB, we do not observe this faceting in the APT data. This is likely due to the field-of-view of APT that is smaller compared to the TKD, i.e. the signal from the TKD comes primarily from the bottom part of the specimen, while the APT images from its core. The composition profile across the identified ∑3 TB in Fig. 3 g) exhibits no chemical fluctuations of the matrix elements at the interface. We observe only slightly different In and S compositions for the adjacent grains. Moreover, comparing the Na composition with its background signal ('Na-bg' in Fig. 3 g)) we do not observe any segregation of Na directly at the ∑3 TB. We only detect an enrichment of Na in clusters on the right-hand side of the composition profile.

In addition to RHAGBs and TBs, we identified in another APT dataset a two-dimensionally confined extended defect, likely a stacking fault, as shown in Fig. 4. Besides Na clusters, the Na distribution maps in Fig. 4 c-d) shows an enrichment of Na in a confined planar region, which also exhibit a Cu enrichment compared to the grain interior marked by the blue 26 at.% Cu iso-composition surface. In order to avoid mistaking one of the ∑3 TBs identified by TKD (see Fig. 4 b)) for a stacking fault in the APT dataset, we compared the Na distribution and point density maps in Fig. 4 e-f) of an enlarged section (red dashed line), where all three ∑3 TBs are expected to be located. Fluctuations of the point density in APT are commonly observed at grain boundaries and other crystalline defects, and are related to aberrations in the ions trajectories [23,24]. Two out of the three ∑3 TBs can be clearly identified as planes with higher atomic density marked by red arrows in Fig. 4 f). Their distance to the apex of the APT specimen as well as their spacing, i.e. ~350 nm, ~500 nm, and ~150 nm, respectively, fits with the corresponding distances of the two lower ∑3 TBs in the TKD analysis. For the upper ∑3 TB such a clear correlation is impeded since a heating up of the APT specimen during laser pulsing in this region interferes with the higher atomic density of the ∑3 TB. Nevertheless, between both lower ∑3 TBs there is an approx. ~30 nm thin area, which has a lower atomic density than its surrounding, which can be likely assigned to a stacking fault. A composition profile across this stacking fault in Fig. 4 g) reveals Cu enrichment as well as In and S depletion at the interface. Moreover, the Gibbsian interfacial excess for Na and C are calculated to be $\Gamma_{Na} = 0.09$ atoms/nm^2 and $\Gamma_C = 0.02$ atoms/nm^2, respectively.

In total two RHAGBs, one ∑9 TB and eight ∑3 TBs as well as one stacking fault were analyzed. The corresponding chemical fluctuations at these extended defects are listed in Table 3. At all RHAGBs, the ∑9 TB and the stacking fault we detect Cu enrichment as well as In depletion and for the vast majority S depletion as well. Moreover, we observe for these defects co-segregation of Na and C, except for the ∑9 TB, which only shows segregation of C. We do not detect any segregation of K or O atoms at RHAGBs and ∑9 TB in the Cu-rich $CuInS_2$ sample. The calculated Gibbsian excess values for Na and C varies from defect to

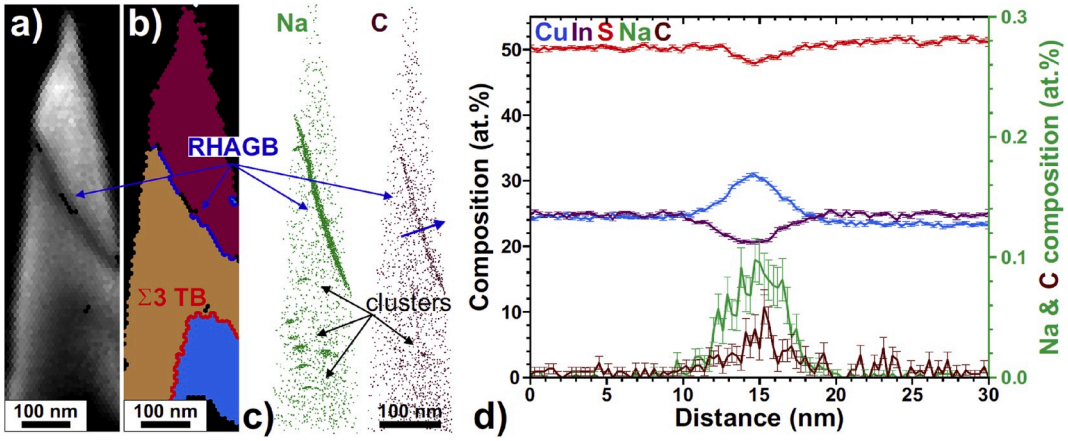

Fig. 2. a-b) IQ and unique colour map from an APT needle from the Cu-rich sample showing a RHAGB (blue) with a misorientation angle of 26.4° @ [1 1 0] as well as a ∑3 TB (red). Only data points with a confidence index (CI) > 0.1 are shown. c) APT reconstruction showing the Na and C distribution. d) 1D composition profile across the RHAGB (blue arrow) shown in c).

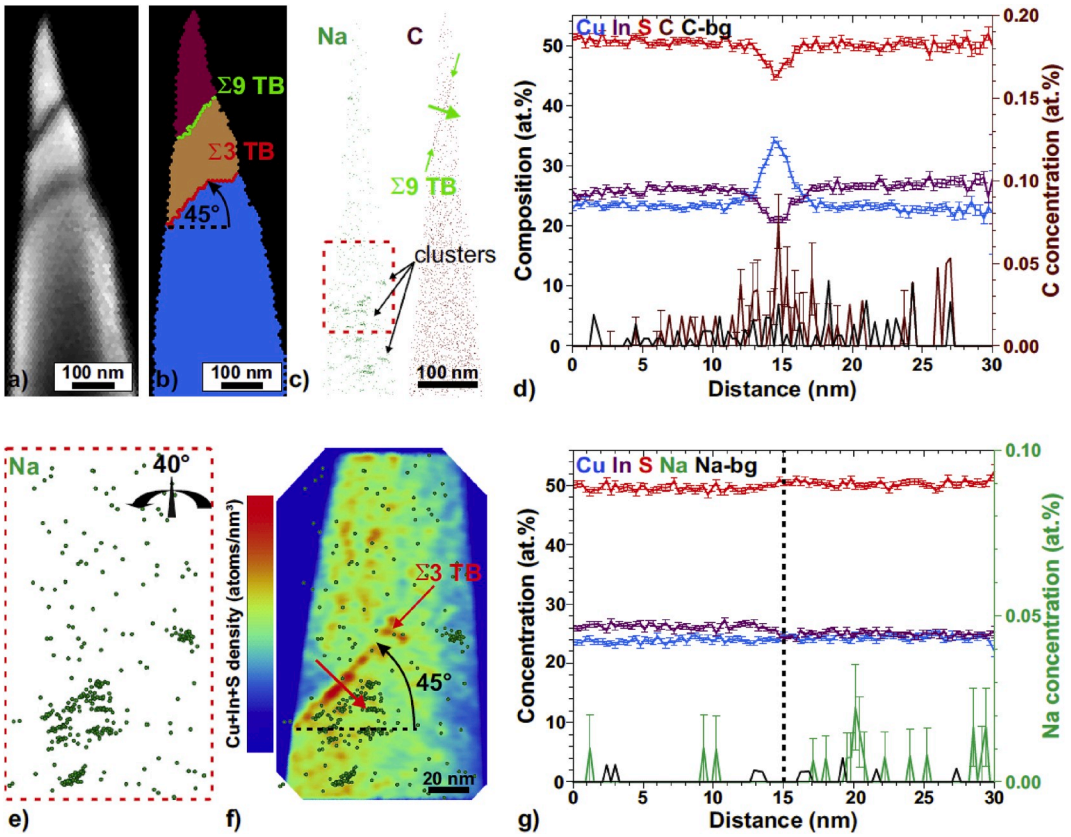

Fig. 3. a-b) IQ and unique colour map from an APT needle from the Cu-rich sample showing one ∑9 TB (green) and one facetted ∑3 TB (red). Only data points with CI > 0.1 are shown. c) APT reconstruction showing the Na and C distribution. d) 1D composition profile across the ∑9 TB (green arrow) shown in c). "C-bg" stands for C background. e) Magnified Na distribution from the red-dashed region in c). The APT dataset was rotated by 40 °C w.r.t. c), i.e. the same orientation as the TKD dataset. f) 2D point density map to e) projected to the plane perpendicular to the viewing direction, which is superimposed with Na atoms. g) 1D composition profile across the ∑3 TB (red arrow) shown in f). The dashed line marks the position of the ∑3 TB. "Na-bg" stands for Na background.

defect, and on average the excess value of Na is five times higher than that of C. In contrast, for all eight ∑3 TBs we do not observe any chemical fluctuations or segregation phenomena. In the grain interior the composition for Na and C varies from 2 ppm to 11 ppm and from 5 ppm to 13 ppm, respectively, suggesting similar solubility for both impurities. In addition, the grains have a Cu-poor composition, where the [Cu]/[In] ratio varies from 0.90 to 0.97.

3.3. *Cu-poor $CuInS_2$ thin-films*

Fig. 5 a-b) show TKD analyses from an APT specimen from the Cu-poor sample. The reconstructed APT dataset in Fig. 5 c) clearly reveals co-segregation of Na and K at the RHAGB (blue line) having a misorientation angle of 49.5° @ [21 8 18]. From the composition profile across this RHAGB in Fig. 5 d) the excess values for Na and K are calculated to be Γ_{Na} = 1.59 atoms/nm^2 and Γ_K = 0.11 atoms/nm^2, respectively. Furthermore, we observe Cu depletion and enrichment of In and S at the RHAGB. Interestingly, the chemical enrichments and depletions show a rather W-shape like profile than a Gaussian shape. We detect as well the same W-shape like composition profile of the chemical fluctuations across some of the SFs. One example is given in Fig. 5 f) for the composition profile of the SF, which is marked by the blue 19 at.% Cu iso-composition surface in Fig. 5 e).

For another specimen given in Fig. 6 the TKD analysis reveals one ∑3 TB and one RHAGB. Besides Na and K segregation, we also detect O at the RHAGB. The composition profile across the RHAGB in Fig. 6 d) reveals that there is no S enrichment at the RHAGB in contrast to that of the previous APT dataset, which exhibit no O segregation at the RHAGB. Furthermore, Cu depletion as well as In enrichment at the RHAGB in Fig. 6 d) are not as clear as for the RHAGB in Fig. 5 d) (see Fig. S4 in supplementary material). Moreover, the composition profile of the matrix elements exhibit no W-like shape at the RHAGB. In the region of the ∑3 TB (red dashed lines), we observe Na decorated linear features, likely dislocations, as displayed in Fig. 5e) and f). However, the ∑3 TB itself shows neither segregation of impurities nor fluctuations of the matrix elements as shown in Fig. 5 g). Slight Cu depletions in the Na-enriched regions around 40 nm and 80 nm within the composition profile are due to the presence of dislocations, which can exhibit Cu depletion (cf. Table 3).

The Cu-poor $CuInS_2$ thin-film shows a high density of dislocations and stacking faults, which is reflected as well in APT measurements. One example how complex the interplay between RHAGBs, stacking faults and dislocations can be is given in Fig. 7. The Na distribution of an APT sub-dataset in Fig. 7 a-b) shows that two linear features, likely dislocations decorated by Na, are connecting two RHAGBs (see Fig. S5 in supplementary material for TKD analysis). However, a closer look to Fig. 7 c) reveals that one 2D confined feature, likely a stacking fault, is running from one RHAGB to the other one, whereby the Na decorated dislocations confine the stacking fault. Moreover, there is a 3D confined region of Cu accumulation at the one end, where the stacking fault is meeting the RHAGB (side-view in Fig. 7 c)). A Na decorated dislocation surrounds part of this region. The 2D compositional maps of Cu from different views are exhibiting complex chemical fluctuations at these defects. 2D compositional maps of In and S as well as composition profiles obtained across the defects can be found in Fig. S6 and Fig. S7 in the supplementary material.

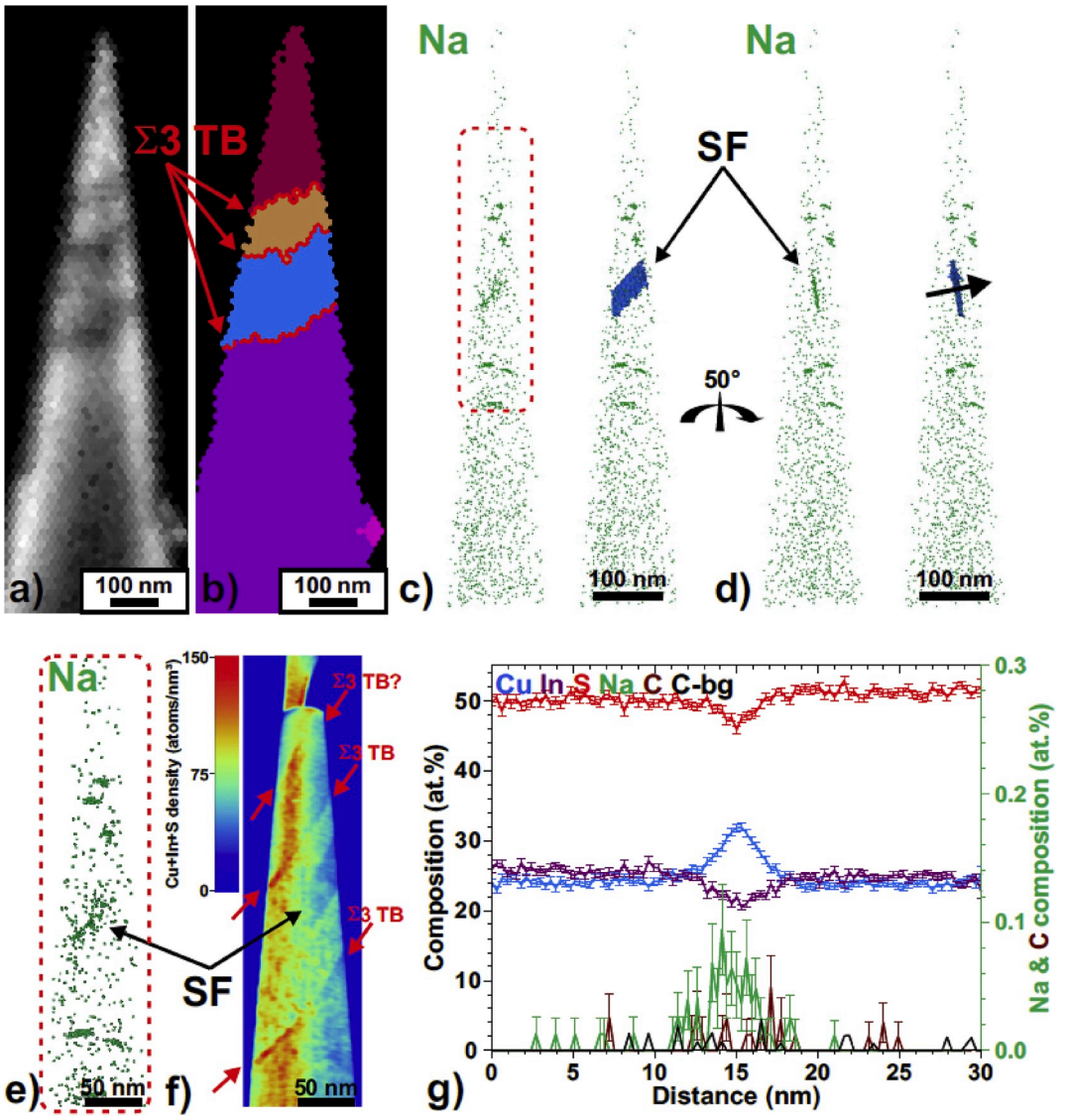

Fig. 4. a)-b) IQ and unique colour map from an APT specimen from the Cu-rich sample showing three $\sum$3 TBs (red). Only data points with CI > 0.1 are shown. c) APT reconstruction showing the Na distribution and a 26 at.% Cu iso-composition surface, which marks a SF. d) Rotated APT dataset by 40° w.r.t. c) showing the 2D confined SF. e) Magnified Na distribution from the red-dashed region in c). f) 2D density map to e) projected to the plane perpendicular to the viewing direction. The upper right region shows a void within the dataset. g) 1D composition profile across the SF (black arrow) shown in d). "C-bg" stands for C background. The reader is referred to the supplementary material to see that there is indeed segregation of C.

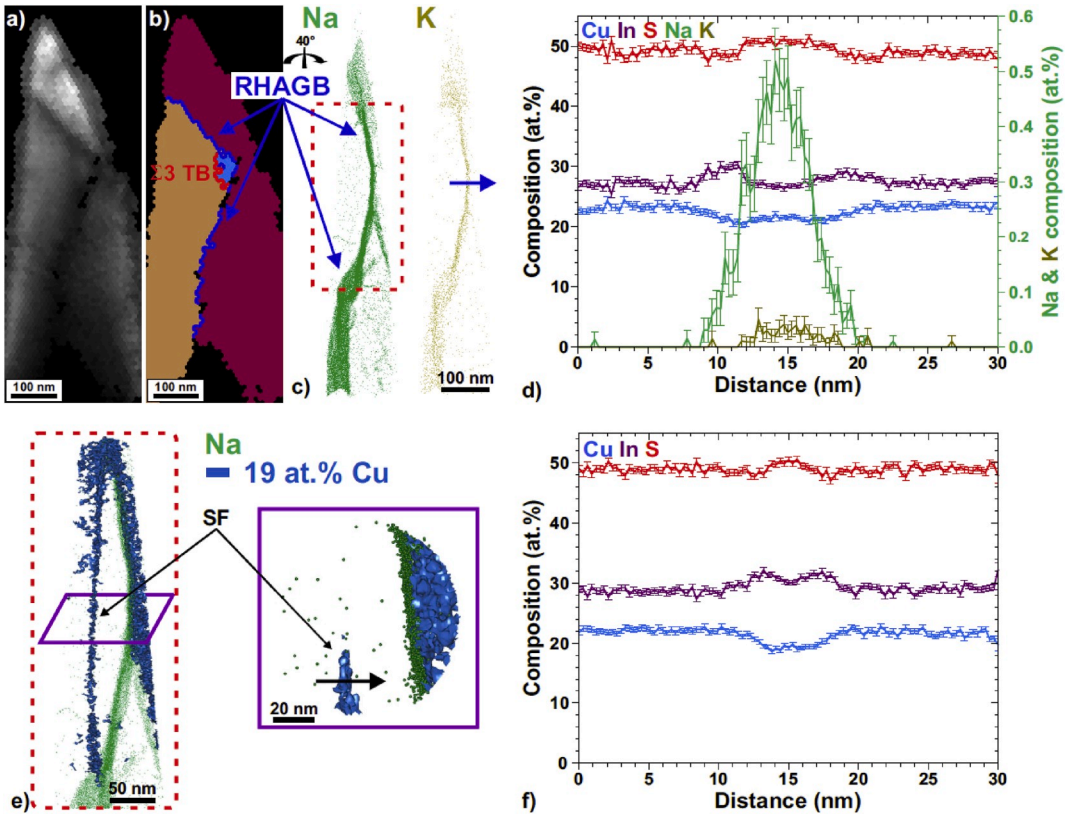

Fig. 5. a)-b) IQ and unique colour map from an APT needle from the Cu-poor sample showing one ∑3 TB (red) and a RHAGB (blue) with a misorientation angle of 49.5° @ [21 8 18]. Only data points with CI > 0.1 are shown. c) APT reconstruction showing the Na and K distribution. d) 1D composition profile across the RHAGB (blue arrow) shown in c). e) Magnified region from the red-dashed region in c) showing the Na distribution and a 19 at.% Cu iso-composition surface as well as the detail of the of SF next to the RHAGB marked by the purple frame. f) 1D composition profile across the SF (black arrow) shown in e).

The chemical fluctuations for all detected RHAGBs, ∑3 TBs, stacking faults and dislocations of the Cu-poor $CuInS_2$ thin-film are listed in Table 3. All RHAGBs show Cu depletion as well In enrichment. For S we cannot observe any clear trend since we detect enrichment, depletion as well as no fluctuation. Moreover, at almost all RHAGBs we observe segregation of Na, K and O. On average the Gibbsian interfacial excess values of Na are one order of magnitude higher than that of K and five times higher than that of O. In the grain interior the composition for Na and K varies from 7 ppm to 23 ppm and from 2 ppm to 11 ppm, respectively. The composition of O in the grain interior was not calculated as we cannot distinguish between O coming from the APT specimen and its background signal, i.e. residual gases in the APT analysis chamber. In addition, the grains reveal a Cu-poor composition, where the [Cu]/[In] ratio varies from 0.73 to 0.97.

In contrast to RHAGBs, both ∑3 TB exhibit neither chemical fluctuations nor segregation phenomena. The majority of the stacking faults show the same chemical fluctuations as the RHAGBs, i.e. Cu depletion and In enrichment. Only in some cases we observe Cu enrichment and In depletion. Moreover, in contrast to the RHAGBs we do not detect any segregation of impurities at stacking faults. The dislocations do not show any clear trend. One half shows no chemical fluctuations, whereas for the other half we observe Cu depletion and In enrichment. As for the RHAGBs and stacking faults, there is no clear trend for S at dislocations. All dislocations are decorated by Na atoms but only a small fraction by K atoms.

4. Discussion

4.1. Relationship between chemistry and structure of extended defects

According to Table 3, an atomic redistribution of the matrix elements takes place at RHAGBs in both the Cu-rich and the Cu-poor $CuInS_2$ thin-film. For the latter one we find a 'In on Cu' scenario at RHAGBs, i.e. Cu depletion and In enrichment. This scenario indicates that also for Cu-poor sulfide based chalcopyrites, here $CuInS_2$, the formation of In_{Cu} and V_{Cu} point defects pair might take places at RHAGBs similar to selenide based Cu-poor Cu(In,Ga)Se_2 thin-films [16–18]. Our findings are in good agreement with *ab initio* density functional theory calculations, which show that In_{Cu} and V_{Cu} point defects have the lowest formation energies for Cu-poor and In-rich $CuInS_2$ [25,26]. For S we observe no clear trend. Furthermore, the compositional fluctuations at RHAGBs are always accompanied by co-segregation of Na and K as well as in most cases of O. According to several groups [16–18], O segregation at RHAGBs in Se-based Cu(In,Ga)Se_2 thin-films occurs only if there is a depletion of Se or no change in Se composition at the interface, i.e. the absence of Se enrichment. Our APT measurements confirms that this applies as well for the vast majority of RHAGBs in Cu-poor $CuInS_2$ thin-films. Moreover, the Gibbsian interfacial excess values of Na are up to one order of magnitude larger than those of K. This can be explained by the different amounts of Na_2O and K_2O in the SLG substrate, which are 14 at% and approx. 0.4 at%, respectively. Since the ratio of Gibbs excess values between Na and K is similar to the ratio of their amount in the SLG substrate, the diffusion coefficients of Na and K in $CuInS_2$ thin-films are similar like it was observed for selenide based thin films [27].

In contrast, for the Cu-rich $CuInS_2$ thin-films we observe a 'Cu on In' scenario at RHAGB and at one ∑9 TB, i.e. In depletion and Cu enrichment. This scenario indicates that for Cu-rich $CuInS_2$ thin-films the formation of Cu_{In}, $Cu_i$and V_{In} point defects may take places at RHAGBs. Our findings are in good agreement with *ab initio* density functional theory calculations, which show that Cu_{In}, Cu_ias well as V_{In}point defects have the lowest formation energies for Cu-rich and In-poor $CuInS_2$ [25,

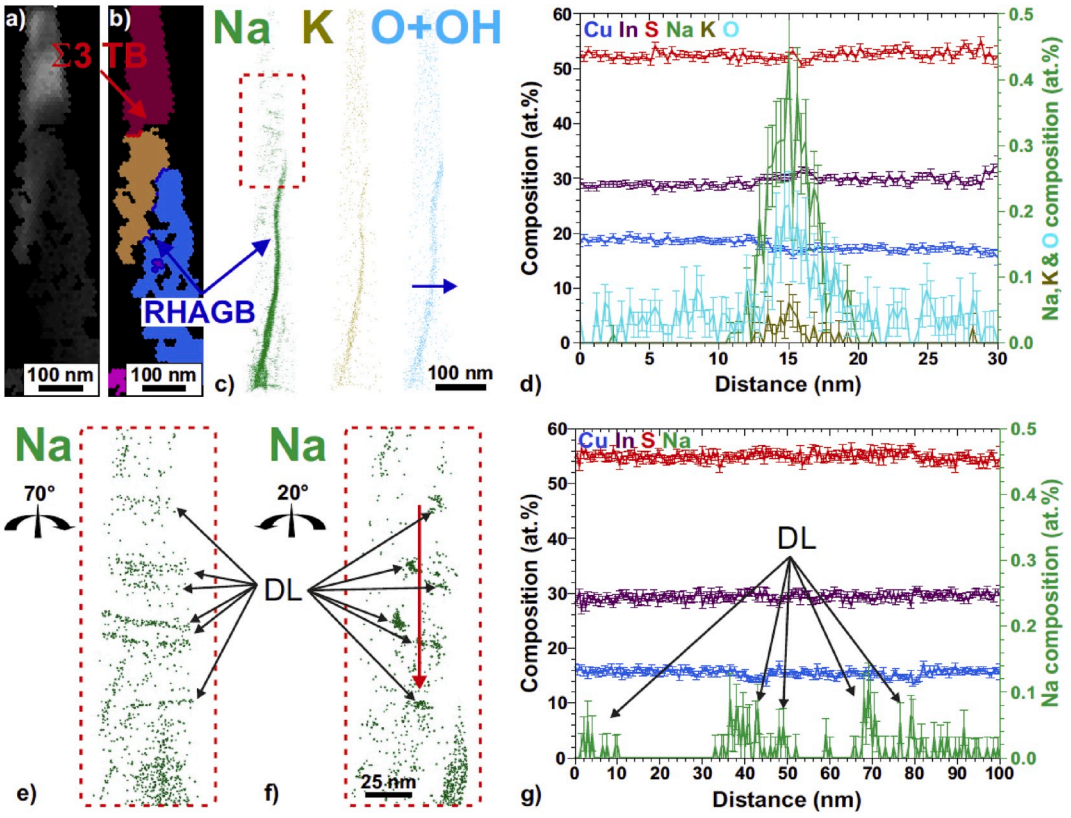

Fig. 6. a)-b) IQ and unique colour map from an APT needle from the Cu-poor sample showing one ∑3 TBs (red) and a RHAGB (blue) with a misorientation angle of 40.8° @ [5 4 14]. Only data points with CI > 0.1 are shown. c) APT reconstruction showing the Na, K, and O & OH distribution. d) 1D composition profile across the RHAGB (blue arrow) shown in c). e) and f) magnified region from different views from the red-dashed region in c) showing the Na distribution within the expected region for the ∑3 TB. g) 1D composition profile across the expected position of the ∑3 TB (red arrow) shown in f). There are several Na decorated linear defects within this region, likely dislocations as marked by DL.

26]. Cu-enriched RHAGBs were also found in selenide based Cu(In,Ga)Se_2 thin-films, which had an intermediate Cu-rich growth step but where the final overall film composition was Cu-poor and Ga-rich [28]. Interestingly, the compositional fluctuations at RHAGBs in Cu-rich $CuInS_2$ thin-film are always accompanied by co-segregation of Na and C but not by K and O as for the Cu-poor $CuInS_2$ thin-films. This also true for a ∑9 TB, where only segregation of C is found but not of K and O. The absence of K might be related to a larger grain size and a significantly reduced density of dislocations, which can interconnect the grains (cf. Figs. 1 g) and Fig. 7), in the Cu-rich $CuInS_2$ thin-film compared to the Cu-poor one. Since the diffusivity of elements along dislocations is in general faster than along RHAGBs and through the bulk [29], smaller Gibbsian excess values of Na and K can be expected at RHAGBs in the Cu-rich $CuInS_2$ thin-film. Indeed, the Gibbsian excess values of Na in the Cu-rich sample are almost by one order of magnitude lower than those in the Cu-poor sample (see Table 3). Furthermore, the amount of K in the SLG substrate is more than one order of magnitude smaller than the amount of Na. Therefore, the expected Gibbsian excess value for K at RHAGBs in the Cu–rich $CuInS_2$ film is in the range of 0.001–0.01 atoms/nm^2, which is in the range of the detection limit of the APT technique. The absence of O at RHAGBs is not clear. According to Kronik et al. [30] there is an oxidation-catalysis effect of Na, i.e. if there is less Na at RHAGBs there should be also less O. However, this cannot completely explain the absence of O. Given the facts that the Gibbsian excess value of O can be twice as high as that of K in the Cu-poor sample and that the amount of O is even two orders of magnitudes higher than that of K in the SLG substrate, we would still expect a detectable segregation effect of O in the Cu-rich sample. Another possible explanation is that the C-enriched environment at RHAGBs might be energetically unfavorable for O.

In contrast to RHAGBs and Σ9 TBs, we do not detect any compositional fluctuations at Σ3 TBs. This agrees with findings in Cu(In,Ga)Se_2 thin-films [17,18]. According to Abou-Ras et al. [31], our observations suggests that those Σ3 TBs consist of cation-S-terminated {112} interface planes. The absence of impurity segregation at Σ3 TBs indicates that they are coherent, i.e. the bonding across the interface is not disrupted, which makes impurity segregation unlikely [32]. However, although all investigated Σ3 TBs show no impurity segregation, we cannot exclude segregation phenomena at Σ3 TBs in general. Indeed, TKD analyses (see Fig. 3 b)) reveal that one APT dataset of the Cu-rich $CuInS_2$ sample contains an incoherent Σ3 TB with facets and ledges. Therefore, segregation of impurities can be locally possible, but as shown in Fig. 3 e-f) these structural features might not be detected within the limited field of view of the APT technique. High-resolution (HR) (S)TEM measurements may help to resolve whether facetted Σ3 TBs show induced strain at the facet junctions or not.

The vast majority of stacking faults in both Cu-rich and Cu-poor $CuInS_2$ samples seems to show similar chemical fluctuations as the RHAGBs. While we observe Na and C segregation at the stacking fault in the Cu-rich $CuInS_2$ sample, we do not detect any segregation of impurities at stacking faults in the Cu-poor one. This observation may be related to a certain type of stacking fault structure, which seems to be energetically unfavorable for impurity segregation [33]. Therefore, correlated high-resolution TEM-APT measurements are needed to resolve the atomic structures of the different stacking fault types and to compare them with their chemistry. In contrast to RHAGBs and stacking faults, dislocations do not show any clear picture.

At some RHAGBs as well as stacking faults in the Cu-poor $CuInS_2$ thin-film we observe a W-like profile of the chemical fluctuations of the

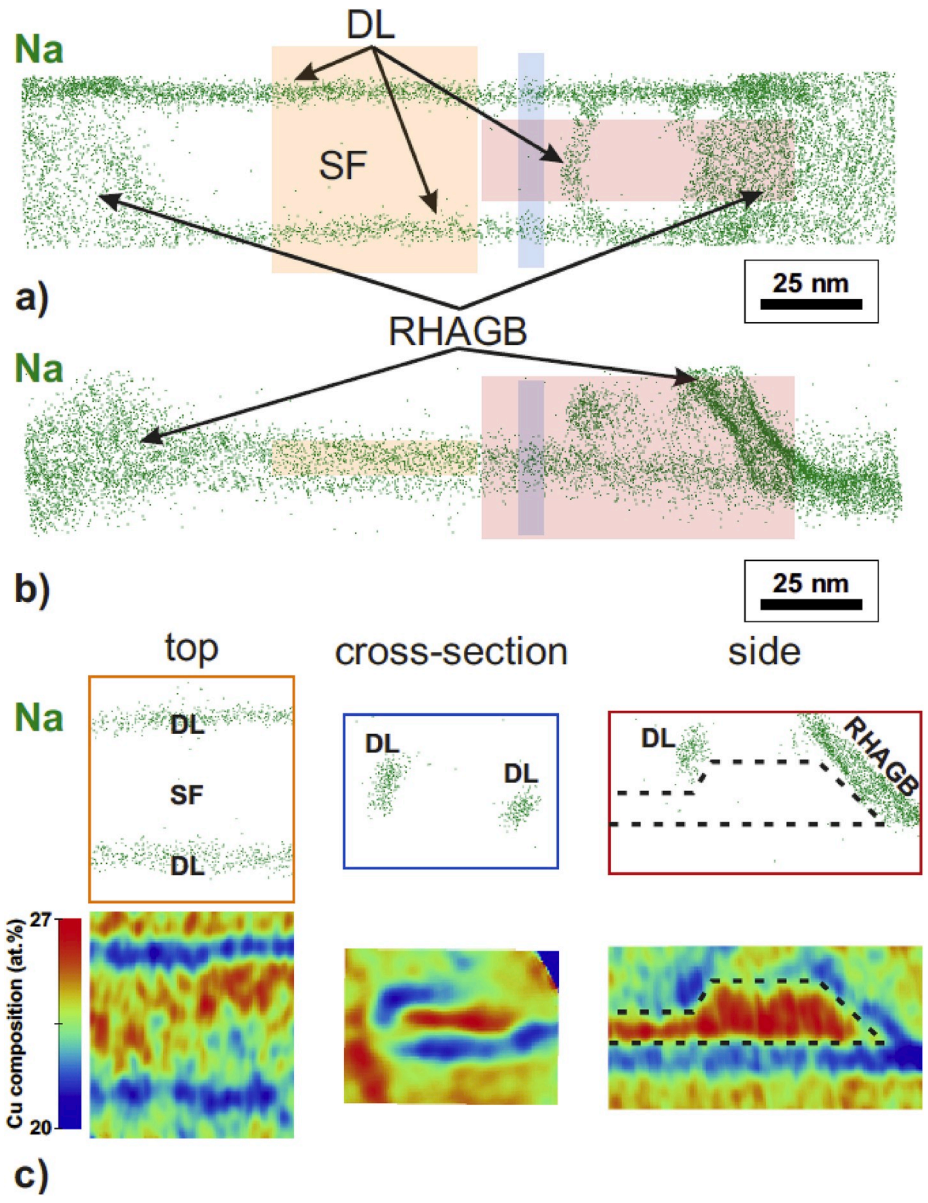

Fig. 7. a)-b) Na distribution of an APT dataset of the Cu-poor sample in top and side view showing a network of RHAGBs, SFs and dislocations (DL). c) Na distribution and 2D compositional Cu map in top, cross-section and side view of the highlighted regions (orange, blue, red) in c).

matrix elements, especially for In and Cu (see Fig. 5). This is not due to local magnification effects (see Fig. S8 in supplementary material for more information), which is a well-known artifact in APT measurements [34]. The origin of this shape might be that at an early stage of the film growth some of the RHAGBs and stacking faults were highly enriched with In on Cu sites, which may be energetically unfavorable compared to a lower In enrichment observed in the final grown sample. During further film growth Cu atoms diffuse from the grain interior towards the interfaces and kick-out In atoms and reoccupy their original Cu sites leading to a W-like chemical profile. Another possible explanation is that defects with a W-like profile have an extended complex atomic arrangement, which needs to be elucidated by complementary HR-(S) TEM.

It should be noted that, although we only observe Cu depletion at RHAGBs and at the vast majority of the SFs in the Cu-poor CIS thin-film, we cannot exclude the presence of Cu enrichment at some RHAGBs. The [Cu]/[In] ratio of the Cu-poor CIS film is with 0.95 close to stoichiometry and the observed Cu enrichment at some SFs and dislocations (see Table 3) indicates that a small part of RHAGBs may exhibit Cu enrichment similar to findings of Simsek Sanli et al. [35] for the Cu-poor selenide system. For the Cu-rich CIS thin-film one may expect that there exist no RHABGs with Cu depletion since the formation energies of In_{Cu} and V_{Cu} point defects are very high due to the [Cu]/[In] ratio of 1.83. However, excess Cu leads to the formation of Cu-S secondary phases (see Fig. 1 b)) and, hence, locally the chemical environment may favor also Cu-depleted RHAGBs.

4.2. Possible effects of the chemistry and structure of extended defects on the device performance

A discussion of possible effects of the above observations on the solar cell properties is difficult due to the complex segregation phenomena and their interaction with the chemical fluctuations of Cu, In and S. However, a comparison with the similar selenide based CIGSe system can give first indications.

One can expect an increased defect density at RHAGBs due to disrupted bonds. However, DFT calculations of the selenide compounds suggest that the density of deep defects is not significantly increased, i.e.

Table 3
Chemical composition changes at defects in Cu-rich and Cu-poor $CuInS_2$ thin-film. +, -, o corresponds to enrichment, to depletion, and to no change, respectively.

Defect type	Cu	In	S	Γ_{Na} (at/nm^2)	Γ_C (at/nm^2)	Γ_K (at/nm^2)	Γ_O (at/nm^2)
Cu-rich $CuInS_2$ thin-film							
26.4°@[110]	++	–	–	0.17	0.05	–	–
RHAGB	+	–	o	0.31	0.05	–	–
∑9 TB	++	–	–	–	0.03	–	–
1x SF	++	–	–	0.09	0.02	–	–
8x ∑3 TB	o	o	o	–	–	–	–
Cu-poor $CuInS_2$ thin-film							
49.5° @ [21 8 18]	–	+	+	1.59	–	0.11	–
40.8° @ [5 4 14]	–	+	o	0.63	–	0.06	0.23
44.2° @ [18 9 5]	–	+	o	0.94	–	0.15	0.17
57.4° @ [19 12 3]	–	+	–	3.44	–	0.18	0.60
RHAGB	–	+	+	1.78	–	0.20	0.24
5x SF	–	+	o	–	–	–	–
4x SF	–	+	+	–	–	–	–
3x SF	–	+	–	–	–	–	–
1x SF	–	o	+	–	–	–	–
3x SF	o	++	–	–	–	–	–
3x SF	+	–	+	–	–	–	–
1x SF	+	o	–	–	–	–	–
2x ∑3 TB	o	o	o	–	–	–	–
Dislocations				**Na (at. %)**	**C (at. %)**	**K (at. %)**	**O (at. %)**
10x	o	o	o	0.2-0.7	–	–	–
3x	–	o	o	0.4-0.8	–	–	–
4x	–	o	+	0.2-0.8	–	0-0.03	–
3x	–	+	o	0.5-1.2	–	0-0.03	–
1x	–	+	+	0.4	–	–	–
1x	–	+	–	0.2	–	–	–
1x	+	–	+	0.2	–	–	–
1x	+	–	o	0.2	–	–	–

the created defects are rather shallow [36,37]. This is related to an atomic redistribution, which leads to a relaxation of deep defects [31]. Table 3 clearly reveals that such an atomic redistribution might also takes place at RHAGBs and ∑9 TBs in $CuInS_2$ thin-films. For the Cu-poor $CuInS_2$ thin-film one can expect that the Cu depletion leads to a downward bending of the band gap at the RHAGBs since the uppermost valence band of $CuInS_2$ is attributed to Cu-3 d and S-3 p orbitals [25,26]. In addition, DFT calculations on the selenides suggests that the segregation of Na leads to the formation of Na_{Cu} point defects, which reduces the density of In_{Cu} donors [38]. Na_{Cu} point defects do not lead to the formation of additional defect levels within the band gap [38]. Since K is as well an alkali element, we expected similar beneficial effects as for Na. According to Kronik et al. [30], O should passivate detrimental S vacancies. Hence, even though non-radiative recombination takes place at RHAGBs, the therefore caused reduction of the open-circuit voltage V_{OC} of the final device can be limited by the above-mentioned mechanisms to a certain extend.

DFT calculations by Yang et al. [26] suggest that a Cu enrichment as we observe at RHAGBs and ∑9 TBs in the Cu-rich $CuInS_2$ thin-film and to some extend at SFs in the Cu-poor $CuInS_2$ thin-film may lead to a band gap narrowing. The effect of segregation of Na and in particular that of C at these Cu-enriched defects is unclear due to the lack of related theoretical calculations. Hence, whether such a band gap narrowing indeed exist and how Na and C affect the optoelectronic properties needs to be investigated by techniques such as Kelvin probe force microscopy (KPMF) and cathodoluminescence (CL). Furthermore, for the Cu-rich $CuInS_2$ thin-film the CdS buffer can penetrate deep into the absorber and the highly conductive Cu-S phases [39] can be located close to Cu-enriched RHAGBs (see Fig. 1 and Fig. S2 in SI). Hence, short-circuit paths are easily formed, which are most likely responsible that these Cu-rich $CuInS_2$ absorber yield no working solar cells.

In the case of coherent ∑3 TBs, we do not expect a significant increase of the point defect density, particularly of deep defects, and, hence, no enhanced non-radiative recombination. Therefore, we consider the coherent ∑3 TBs as electrically benign. In contrast, facetted ∑3 TBs (see Fig. 3 b)) give rise to recombination activity since additional strain can be induced due to faceting, which might be compensated by point defects and or linear defects [24].

The above-mentioned mechanisms may be applied as well to stacking faults and dislocations and are not further discussed in detail.

The quasi Fermi level splitting QFLS, which reflects the recombination activities and the quality of the absorber solely, shows that with Cu-rich $CuInS_2$ thin-films one can achieve - in principal - a higher V_{OC} than with Cu-poor $CuInS_2$ thin-films due their higher QFLS (see Table 2). If the shunting problem for the Cu-rich sample and recombination losses at the CdS/$CuInS_2$ interface, which is a typical problem of sulfide based chalcopyrite solar cells [40,41], can be overcome, it is necessary to further increase the QFLS and, hence, the maximum achievable V_{OC}. The work of Lomuscio et al. [14] reveals that the QFLS for $CuInS_2$ is limited by a deep defect around 0.8 eV, which is less present in Cu-rich $CuInS_2$ thin-film. Therefore, it is necessary to annihilate detrimental point defects, dislocations and stacking faults as well as to reduce the grain boundary surface area, as all structural defects might be the origin of this energetically deep defect. This is in particular true for the Cu-poor $CuInS_2$ thin-film, which exhibits a significantly larger density of extended defects compared to the Cu-rich $CuInS_2$ thin-film (see Fig. 1). Furthermore, by reducing the afore-mentioned defects also the strong chemical fluctuations detected at these features are reduced and, hence, related tail states, which leads to an increased QFLS [42]. Therefore, additional annealing steps, especially for Cu-poor $CuInS_2$ thin-films, should help to increase the absorber quality and, hence, the V_{OC}. For Cu-rich $CuInS_2$ thin-films the influence of C on the QFLS needs to be investigated in a future study.

5. Conclusions

We conducted correlated TKD-APT measurements to shed light on the local chemistry of extended defects in Cu-poor and Cu-rich $CuInS_2$ thin-films. At RHAGBs and Σ9 TBs we detect varied chemical fluctuations of the matrix elements, which are accompanied by co-segregation of impurities, whereas at Σ3 TBs we do not observe such phenomena. For the Cu-poor $CuInS_2$ thin-film we observe Cu depletion and In enrichment as well as segregation of Na, K and O. For S we do not observe a clear trend. In contrast, for the Cu-rich $CuInS_2$ thin-film we detect at RHAGBs and Σ9 TBs Cu enrichment and In and S depletion as well as segregation of Na and C. The alkali elements Na and K in both samples originate from the SLG substrate. O may also diffuse-out of the SLG substrate according to the model of Kronik et al. [30]. The source of C in the Cu-rich $CuInS_2$ thin-film is more unclear as it may originate either from a KCN etching step or from the chemical bath deposition of CdS.

The vast majority of stacking faults show similar chemical fluctuations as the RHAGBs in the corresponding $CuInS_2$ thin-film. Interestingly, stacking faults in the Cu-poor $CuInS_2$ thin-film are not accompanied by segregation of impurities, whereas they do in Cu-rich one. To find the origin of this observation, the atomic structure and chemistry of stacking faults needs to be elucidated in future studies. Dislocations are chemically more flexible and show varied compositional fluctuations and are always decorated with Na.

Whether the observed In enrichment and Cu depletion as well as the Cu enrichment and In depletion at RHAGBs in the Cu-poor and Cu-rich $CuInS_2$ samples, respectively, may lead to an atomic reconstruction and may serve as a passivation effect needs to be elucidated in future studies like by KPFM and CL measurements. Furthermore, CdS can protrude deep into the bulk of the Cu-rich $CuInS_2$ sample and Cu-S phases, which

are highly conductive, can be located close to these Cu-enriched defects, which can easily build up short-circuit paths and, hence, lead to non-working solar cells. The absence of compositional fluctuations and segregation phenomena at highly symmetric Σ3 TBs indicates that the point defect density is not substantially increased at this type of defect.

Declaration of competing interest

The authors declare that they have no known competing financial interests or personal relationships that could have appeared to influence the work reported in this paper.

CRediT authorship contribution statement

Torsten Schwarz: Investigation, Formal analysis, Conceptualization, Visualization, Writing - original draft, Funding acquisition. **Alberto Lomuscio:** Investigation, Formal analysis, Writing - review & editing. **Susanne Siebentritt:** Conceptualization, Writing - review & editing, Funding acquisition. **Baptiste Gault:** Conceptualization, Writing - review & editing, Funding acquisition.

Acknowledgements

The authors are grateful to Uwe Tezins, Andreas Sturm, Christian Broβ, and Volker Kree for their support to the APT, SEM, FIB, and TEM facilities at Max-Planck-Institut für Eisenforschung GmbH. This work was supported by the German Research Foundation (DFG) (Contract GA 2450/1-1) and by the Luxembourgish Fonds National de la Recherche (CORRKEST).

Appendix A. Supplementary data

Supplementary data to this article can be found online at https://doi.org/10.1016/j.nanoen.2020.105081.

References

[1] A.D. Vos, Detailed balance limit of the efficiency of tandem solar cells, J. Phys. Appl. Phys. 13 (5) (1980) 839–846.
[2] R. Scheer, H.W. Schock, Chalcogenide Photovoltaics: Physics, Technologies, and Thin Film Devices, Wiley-VCH Verlag GmbH & Co. KGaA, Weinheim, 2011.
[3] H. Hiroi, Y. Iwata, S. Adachi, H. Sugimoto, A. Yamada, New world-record efficiency for pure-sulfide Cu(in,Ga)S2 thin-film solar cell with Cd-free buffer layer via KCN-free process, IEEE J. Photovolt. 6 (3) (2016) 760–763.
[4] Y.K. Nakamura M, Y. Kimoto, Y. Yasaki, T. Kato, H. Sugimoto, Cd-free Cu (In,Ga)(Se,S)2 thin-film solar cell with a new world recordefficacy of 23.35%, in: 46th IEEE PVSC, 2019. Chicago, IL.
[5] R. Carron, S. Nishiwaki, T. Feurer, R. Hertwig, E. Avancini, J. Löckinger, S.C. Yang, S. Buecheler, A.N. Tiwari, Advanced alkali treatments for high-efficiency Cu(in,Ga)Se2 solar cells on flexible substrates, Adv. Energy Mater. 9 (24) (2019).
[6] T.M. Friedlmeier, P. Jackson, A. Bauer, D. Hariskos, O. Kiowski, R. Menner, R. Wuerz, M. Powalla, High-efficiency Cu(In,Ga)Se2 solar cells, Thin Solid Films 633 (2017) 13–17.
[7] P. Jackson, D. Hariskos, R. Wuerz, W. Wischmann, M. Powalla, Compositional investigation of potassium doped Cu(In,Ga)Se2 solar cells with efficiencies up to 20.8%, Phys. Status Solidi Rapid Res. Lett. 8 (3) (2014) 219–222.
[8] I. Hengel, A. Neisser, R. Klenk, M.C. Lux-Steiner, Current transport in CuInS2:Ga/Cds/Zno – solar cells, Thin Solid Films 361–362 (2000) 458–462.
[9] R. Klenk, Characterisation and modelling of chalcopyrite solar cells, Thin Solid Films 387 (1–2) (2001) 135–140.
[10] A. Ennaoui, M. Bär, J. Klaer, T. Kropp, R. Sáez-Araoz, M.C. Lux-Steiner, Highly-efficient Cd-free CuInS2 thin-film solar cells and mini-modules with Zn(S,O) buffer layers prepared by an alternative chemical bath process, Prog. Photovoltaics Res. Appl. 14 (6) (2006) 499–511.
[11] S. Merdes, R. Sáez-Araoz, A. Ennaoui, J. Klaer, M.C. Lux-Steiner, R. Klenk, Recombination mechanisms in highly efficient thin film Zn(S,O)/Cu(In,Ga)S2 based solar cells, Appl. Phys. Lett. 95 (21) (2009).
[12] A. Lomuscio, M. Melchiorre, S. Siebentritt, Influence of stoichiometry and temperature on quasi Fermi level splitting of sulfide CIS absorber layers, in: IEEE 7th World Conference on Photovoltaic Energy Conversion (WCPEC) (A Joint Conference of 45th IEEE PVSC, PVSEC & 34th EU PVSEC), 2018, pp. 1922–1924, 2018.
[13] S. Fiechter, Y. Tomm, M. Kanis, R. Scheer, W. Kautek, On the homogeneity region, growth modes and optoelectronic properties of chalcopyrite-type CuInS2, Phys. Status Solidi 245 (9) (2008) 1761–1771.
[14] A. Lomuscio, T. Rödel, T. Schwarz, B. Gault, M. Melchiorre, D. Raabe, S. Siebentritt, Quasi-fermi-level splitting of Cu-poor and Cu-rich CuInS2 absorber layers, Phys. Rev. Appl. 11 (5) (2019), 054052, https://doi.org/10.1103/PhysRevApplied.11.054052.
[15] S. Siebentritt, What limits the efficiency of chalcopyrite solar cells? Sol. Energy Mat. Sol. C 95 (6) (2011) 1471–1476.
[16] D. Abou-Ras, B. Schaffer, M. Schaffer, S.S. Schmidt, R. Caballero, T. Unold, Direct insight into grain boundary reconstruction in polycrystalline Cu(in,Ga)Se2 with atomic resolution, Phys. Rev. Lett. 108 (7) (2012), 075502.
[17] O. Cojocaru-Mirédin, T. Schwarz, D. Abou-Ras, Assessment of elemental distributions at line and planar defects in Cu(In,Ga)Se2 thin films by atom probe tomography, Scripta Mater. 148 (2017) 106–114.
[18] T. Schwarz, G. Stechmann, B. Gault, O. Cojocaru-Mirédin, R. Wuerz, D. Raabe, Correlative transmission Kikuchi diffraction and atom probe tomography study of Cu(In,Ga)Se2 grain boundaries, Prog. Photovoltaics Res. Appl. 26 (3) (2018) 196–204.
[19] A. Thomere, C. Guillot-Deudon, M.T. Caldes, R. Bodeux, N. Barreau, S. Jobic, A. Lafond, Chemical crystallographic investigation on Cu2S-In2S3-Ga2S3 ternary system, Thin Solid Films 665 (2018) 46–50.
[20] K. Thompson, D. Lawrence, D.J. Larson, J.D. Olson, T.F. Kelly, B. Gorman, In situ site-specific specimen preparation for atom probe tomography, Ultramicroscopy 107 (2–3) (2007) 131–139.
[21] M. Herbig, P. Choi, D. Raabe, Combining structural and chemical information at the nanometer scale by correlative transmission electron microscopy and atom probe tomography, Ultramicroscopy 153 (2015) 32–39.
[22] O.C. Hellman, D.N. Seidman, Measurement of the Gibbsian interfacial excess of solute at an interface of arbitrary geometry using three-dimensional atom probe microscopy, Mater. Sci. Eng., A 327 (1) (2002) 24–28.
[23] C. Oberdorfer, S.M. Eich, G. Schmitz, A full-scale simulation approach for atom probe tomography, Ultramicroscopy 128 (2013) 55–67.
[24] C.H. Liebscher, A. Stoffers, M. Alam, L. Lymperakis, O. Cojocaru-Mirédin, B. Gault, J. Neugebauer, G. Dehm, C. Scheu, D. Raabe, Strain-induced asymmetric line segregation at faceted Si grain boundaries, Phys. Rev. Lett. 121 (1) (2018), 015702.
[25] H. Chen, C.-Y. Wang, J.-T. Wang, X.-P. Hu, S.-X. Zhou, First-principles study of point defects in solar cell semiconductor CuInS2, J. Appl. Phys. 112 (8) (2012), 084513.
[26] P. Yang, L.-J. Shi, J.-M. Zhang, G.-B. Liu, S.A. Yang, W. Guo, Y. Yao, Tuning to the band gap by complex defects engineering: insights from hybrid functional calculations in CuInS2, J. Phys. Appl. Phys. 51 (2) (2017), 025105.
[27] A. Laemmle, Dotierung von Cu(In,Ga)Se2-Schichten mit Natrium und Kalium zur Steigerung des Wirkungsgrads, PhD Thesis, Karlsruher Institut für Technologie (KIT), 2015.
[28] M. Raghuwanshi, E. Cadel, P. Pareige, S. Duguay, F. Couzinie-Devy, L. Arzel, N. Barreau, Influence of grain boundary modification on limited performance of wide bandgap Cu(In,Ga)Se2 solar cells, Appl. Phys. Lett. 105 (1) (2014), 013902.
[29] G. Gottstein, Materialwissenschaft und Werkstofftechnik - Physikalische Grundlagen, 4 ed., Springer Vieweg, Berlin, 2014.
[30] L. Kronik, D. Cahen, H.W. Schock, Effects of sodium on polycrystalline Cu(in,Ga)Se2 and its solar cell performance, Adv. Mater. 10 (1) (1998) 31–36.
[31] D. Abou-Ras, S.S. Schmidt, N. Schäfer, J. Kavalakkatt, T. Rissom, T. Unold, R. Mainz, A. Weber, T. Kirchartz, E. Simsek Sanli, P.A. van Aken, Q.M. Ramasse, H.-J. Kleebe, D. Azulay, I. Balberg, O. Millo, O. Cojocaru-Mirédin, D. Barragan-Yani, K. Albe, J. Haarstrich, C. Ronning, Compositional and electrical properties of line and planar defects in Cu(In,Ga)Se2 thin films for solar cells – a review, Phys. Status Solidi Rapid Res. Lett. 10 (5) (2016) 363–375.
[32] M. Herbig, D. Raabe, Y.J. Li, P. Choi, S. Zaefferer, S. Goto, Atomic-Scale quantification of grain boundary segregation in nanocrystalline material, Phys. Rev. Lett. 112 (12) (2014) 126103.
[33] S.K. Makineni, A. Kumar, M. Lenz, P. Kontis, T. Meiners, C. Zenk, S. Zaefferer, G. Eggeler, S. Neumeier, E. Spiecker, D. Raabe, B. Gault, On the diffusive phase transformation mechanism assisted by extended dislocations during creep of a single crystal CoNi-based superalloy, Acta Mater. 155 (2018) 362–371.
[34] F. Vurpillot, A. Cerezo, D. Blavette, D.J. Larson, Modeling image distortions in 3DAP, Microsc. Microanal.: Off. J. Microsc. Soc. Am., Microbeam Anal. Soc., Microsc. Soc. Canada 10 (3) (2004) 384–390.
[35] E.S. Sanli, Q.M. Ramasse, W. Sigle, D. Abou-Ras, R. Mainz, A. Weber, H.-J. Kleebe, P.A.v. Aken, Elemental redistributions at structural defects in Cu(In,Ga)Se2 thin films for solar cells, J. Appl. Phys. 120 (20) (2016) 205301.
[36] H. Mönig, Y. Smith, R. Caballero, C.A. Kaufmann, I. Lauermann, M.C. Lux-Steiner, S. Sadewasser, Direct evidence for a reduced density of deep level defects at grain boundaries of Cu(in,Ga)Se2 thin films, Phys. Rev. Lett. 105 (11) (2010) 116802.
[37] Y. Yan, R. Noufi, M.M. Al-Jassim, Grain-boundary physics in polycrystalline CuInSe2 revisited: experiment and theory, Phys. Rev. Lett. 96 (20) (2006) 205501.
[38] S.-H. Wei, S.B. Zhang, A. Zunger, Effects of Na on the electrical and structural properties of CuInSe2, J. Appl. Phys. 85 (10) (1999) 7214.
[39] S. Niki, P.J. Fons, A. Yamada, Y. Lacroix, H. Shibata, H. Oyanagi, M. Nishitani, T. Negami, T. Wada, Effects of the surface Cu2−xSe phase on the growth and properties of CuInSe2 films, Appl. Phys. Lett. 74 (11) (1999) 1630–1632.
[40] Y. Hashimoto, K. Takeuchi, K. Ito, Band alignment at CdS/CuInS2 heterojunction, Appl. Phys. Lett. 67 (7) (1995) 980–982.
[41] L. Weinhardt, O. Fuchs, D. Groß, G. Storch, E. Umbach, N.G. Dhere, A.A. Kadam, S. S. Kulkarni, C. Heske, Band alignment at the CdS/Cu(In,Ga)S2 interface in thin-film solar cells, Appl. Phys. Lett. 86 (6) (2005), 062109.
[42] S. Siebentritt, G. Rey, A. Finger, D. Regesch, J. Sendler, T.P. Weiss, T. Bertram, What is the bandgap of kesterite? Sol. Energy Mat. Sol. C 158 (2016) 126–129.

Torsten Schwarz received the diploma in physics in 2011 from the Otto-von-Guericke University of Magdeburg, Germany, and his Ph.D. degree in 2015 from the RWTH Aachen, Germany. During his Ph.D. he investigated chalcopyrite and kesterite based thin-films in the Atom Probe Tomography group at the Max-Planck-Institut für Eisenforschung GmbH (MPIE), Düsseldorf. During 2015–2016 he was a PostDoc at RWTH Aachen. Since 2016 he is a PostDoc at MPIE. His research is focused on the investigation of microstructure-property relationships in materials for photovoltaics, thermoelectrics and polymer electrolyte membrane based fuel cells.

Alberto Lomuscio studied Materials Science and received the B.S. and M.S. degrees from the Aldo-Moro University, Bari in 2013 and Milano-Bicocca University, Milano, Italy, in 2016, respectively. During the Master's thesis, he worked on the deposition of chalcopyrite thin films and solar cells and characterization by Raman spectroscopy. In 2016 he joined the Laboratory of Photovoltaics (LPV) led by Prof. Siebentritt, at University of Luxembourg. At LPV, he is currently working toward the Ph.D degree in optical defect spectroscopy in $CuInS_2$ thin films and solar cells. His research interests include optoelectronic characterization of thin films for photovoltaic applications.

Susanne Siebentritt is a physics professor and heads the laboratory for photovoltaics at the University of Luxembourg. Her research interest is twofold: the electronic structure of semiconductors and thin film solar cells and the fundamental functioning and limitations of these devices. Her interest in thin film solar cells is kindled by the fact that they present the electricity source with the lowest carbon footprint. She is the author of more than 210 peer reviewed publications and an h-index of 40. In 2014 she received the FNR Outstanding Publication Award, together with three co-authors. In 2015 she was awarded the "Grand Prix en Sciences Physique – Prix Paul Wurth" of the Luxembourgish Institut Grand Ducal. She is a board member for the Kopernikus projects, a 10 years research programme for the energy transition of the German Ministry of Education and Research.

Dr Gault leads the Atom Probe Tomography group at the Max-Planck-Institut für Eisenforschung in Düsseldorf and a part-time Reader in Materials at Imperial College London. Since Feb. 2018, he also leads an ERC-Consolidator grant and was the recipient of the 2020 Leibniz Prize. Dr Gault obtained his PhD in physics from the University of Rouen (Feb. 2007). He then held postdoctoral the University of Sydney from 2007 to 2009 and 2010–2012. In between, was Intra-European Marie Curie fellowship at the Department of Materials, University of Oxford. In 2012, he started an academic appointment as Assist. Prof. at McMaster University in Canada.